THERMAL CONDUCTIVITY CHARACTERIZATION OF A CFRP SINGLE-LAP JOINT

Michael Lange [(1)], Volodymyr Baturkin [(2)], Christian Hühne [(1)], Olaf Mierheim [(1)]

[(1)] DLR – German Aerospace Center, Lilienthalplatz 7, 38108, Braunschweig, Germany,
Email: m.lange@dlr.de

[(2)] DLR – German Aerospace Center, Robert-Hooke-Straße 7, 28359 Bremen, Germany,
Email: Volodymyr.Baturkin@dlr.de

KEYWORDS

CFRP, thermal conductivity, joints

ABSTRACT

Fiber reinforced plastics (FRP), especially Carbon-FRPs, are a frequently used material for spacecraft's primary and secondary structural design. Optimal results are achieved when the distinctive orthotropic mechanical properties are considered in the composite structures' design process. Besides their excellent mechanical properties, FRPs offer also a high potential for thermal applications.

In order to allow a partially coupled analysis, Lange [1] proposed a semi-analytic formula which connects the structural and thermal analysis of load-bearing single-lap joints (SLJ). For its validation, a thermal vacuum test was conducted [1] which showed non-conclusive results.

The present paper presents shortcomings identified in [1] and how they are resolved. Next to improvements on the setup an additional experiment on material basis was conducted. It not only allowed the precise confirmation of the calculated CFRP material's thermal conductivity λ_{11}, but also to validate the whole setup for the SLJ experiment. The latest test results revealed that after the implemented setup changes and even though the temperature gradients are strictly limited, the experiment is very sensitive to radiation effects. This is shown by an analytical approximation of the radiative heat loss from the specimen to the environment and comparing it to the experimental results.

1. INTRODUCTION

In [1] Lange simulated and measured the temperature distribution of three carbon fibre-reinforced plastic (CFRP) single-lap joint (SLJ) specimen. The goal was to validate a semi-analytical simulation technique that requires the knowledge of the thermal resistance of the jointed area. It was found that the experimental results do not match the simulation nor they were consistent. Further Lange introduced the analytical implementation on basis of the measurements. The present paper focuses on two major improvements that are related to the measuring setup and specimen preparation. These are:

1) Implementation of two calorimeters (one heater-sided and one sink-sided) in order to measure the actual heat flux in the specimens.
2) The laminate thickness should be significantly enlarged, id est by a factor of ten. This will minimise the specimen's thermal resistance as well as the relative error due to thickness deviations.

In the course of the calorimeter implementation it was also possible to verify for the present paper the material's thermal conductivity. This was in [1] still calculated by the rule of mixture and an assumption made on of the resin's thermal conductivity.

Hence, the paper is sub-divided in two parts. The first one dealing with the thermal conductivity measurement of a single CFRP rod and the second one with the actual SLJ experiment. We will show that even though the temperature gradients are small, radiation plays an important role for the temperature distribution in the given experimental setup and cannot be neglected.

2. IMPROVEMENTS ON SPECIMEN PREPARATION AND TEST SETUP

2.1. Specimen

In [1] it was found that the specimen's laminate thickness t_{lam} requires a significant increase in order to reduce the relative error imposed by thickness variations. This has been realized by manufacturing a laminate with a thickness of t_{lam} = 5 mm and thus an adherend's cross section of A_{rod} = 5x10 mm² for the SLJ specimen. In thickness this is a factor of ten compared to the specimen used before and thus a reduction of the relative thickness error from a range of 10…20% to 1%.

Further only two specimens are investigated in the present study. Firstly, one single CFRP rod (M40J-UD/MTM46, f_{vol}=54%) with the fibres oriented in the longitudinal axis for thermal conductivity verification. Secondly, a single-lap joint is investigated with both adherends featuring the same unidirectional fibre orientation as the rod for the thermal conductivity measurement.

As in [1] the specimen is wrap in single-layer insulation (SLI) foil and housed by an approximated half-spherical shroud to establish together with the

cold plate a homogenous temperature boundary condition.

2.2. Change in test setup

Regarding the test setup two major changes are implemented. The first change relates to the flanges that clamp the CFRP laminates. Before, cf [1], the laminates were glued with the flanges. This results in theory in a very good thermal connection of the laminate and the flanges, but it turned out that the glue distribution was difficult to control and not as precise as intended. Thus, the flanges at cold and warm side were split in two halves and the thermal connection is realized by partial application of thermal conductive pads. …This has also the advantage of general exchangeability between specimen after test as well as using the same flanges for different test purposes (SLJ investigation and thermal conductivity verification).

The most significant change is designated to the implementation of a calorimeter (gSKIN®-XP heat flux meter) in the test setup. This allows the direct measurement of the heat flux into the specimen and therefore a direct comparison to the simulated results. The heat flux meter is added at the warm-sided flange where the heat flux is controlled by the power applied to a resistance heater.

3. THERMAL CONDUCTIVITY VERIFICATION TEST

The goal of the thermal conductivity test is firstly to verify the experimental setup with modified specimen cross section and secondly to confirm the actual thermal conductivity $\lambda_{11} = \lambda_{eff,\,1\text{-}D}$ of the CFRP material used in the later SLJ test. Fig. 1 (top) depicts the specimen with five equidistantly distributed Pt100 sensors (1/3 DIN class B, 3x3x10 mm³ copper housing, 4-wire connection) applied in order to determine an average temperature gradient. The central figure depicts how the rod is clamped at one end with an aluminium flange on the cold plate. At its other end a two-staged flange clamps the rod (detail in bottom of Fig. 1). The first stage S1 clamps the rod itself and the second one S2 contains a heat flux meter (HFM), gSKIN®-XP. On top of the latter flange assembly, a resistance heater (100 Ω) is installed, thus the heat flux runs from the heater through the heat flux meter and the rod towards the cold plate (flange). At each contact interface, the flanges feature a cross section of 10x10 mm², which exactly corresponds to the cross section of the heat flux meter and the width of the rod. The contact resistance is minimized by adding conductive pads (Kerafol® 86/300) at each contact surface.

Further, in order to minimize parasitic heat flux, the second flange stage S2 clamps the sensor via three PA-6 screws and numerous washers. On the other hand, the first stage clamps the rod with stainless screws and both flange parts are connected with aluminium tape, which should allow a homogenous heat flow from top and bottom into the rod. The complete rod, including the Pt100 sensors, is wrapped by an SLI foil (aluminized Mylar®) plus an additional MLI in order to minimize parasitic heat radiation exchange with the cold plate and the shroud, respectively (cf. Fig. 2). The inside surface of the shroud as well as the cold plate are covered by SLI, too. The complete outside surface of the shroud and the cold plate is wrapped by MLI, which minimizes radiative heat exchange with the thermal vacuum chamber. During the test the residual gas pressure in the thermal vacuum chamber is maintained at $p_{chamber} < 5 \cdot 10^{-6}$ mbar.

The scheme in Fig. 3 delineates the temperature sensor positions with respect to the flanges. For the evaluation of the thermal conductivity only temperature sensors $TS_{\#4}$…$TS_{\#9}$ are used. $TS_{\#12}=T_{shroud}$ gives the temperature of the shroud, $TS_{\#13}$ gives the heater temperature and the temperature boundary condition is controlled at the cold plate sensor $TS_{\#14}$. This is maintained at 25°C +/-0.1°C, which is the reference temperature at which the single-lap joint test is conducted, too. The second boundary condition is controlled by the applied heat and the heat flux sensor, respectively. In the current test the heat flux was 704 W/m².

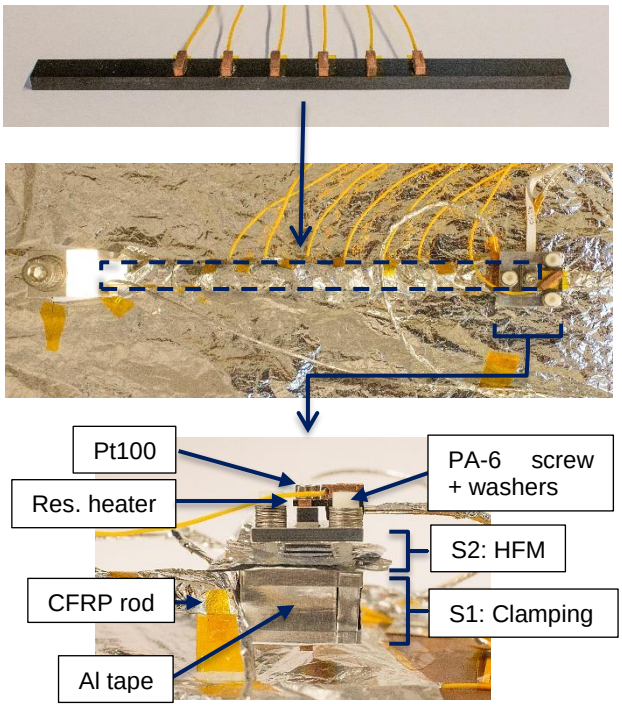

Figure 1: Top: CFRP rod with equidistantly distributed Pt100 sensors; Centre: CFRP rod clamped by cold plate flange (left end) and heater flange incl. heat flux meter (right end), wrapped in SLI (inner MLI, cf Fig.2, not shown); Bottom: Detail of the heater flange.

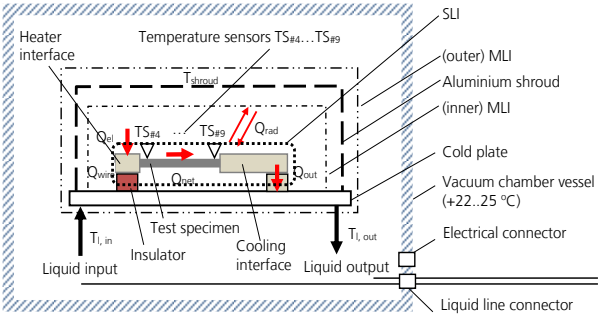

Figure 2: Thermal vacuum setup.

3.1. Estimation of measurement errors

The relative error of longitudinal 1-dimensional heat conductivity is calculated based on the following Eqs. 1-2 for the longitudinal 1-dimensional heat conductivity of sample material $\lambda_{11} = \lambda_{eff,\,1\text{-}D}$:

$$\lambda_{eff,1-D} = Q_{net} \cdot \frac{\Delta L_{sensors}}{\Delta T_{sensors} \cdot F_{cross-sec,\lambda}} \qquad (1)$$

$$Q_{net} = Q_{applied} - \sum_{i=1}^{N} Q_{loss,i} \qquad (2)$$

Here Q_{net} is the heat power at the beginning of the measuring zone (cf sensor #4 in Fig. 3); $Q_{applied}$ is the heat applied to the sample at the base of the heat flux sensor; $Q_{loss,i}$ correspondents to heat losses from the specimen and fixtures to the environment (by wires, via thermal isolation, unsteady components, radiation); $\Delta L_{sensors}$ and $\Delta T_{sensors}$ are the linear distance and temperature difference between the temperature sensors used for heat conductivity measurements; $F_{cross\text{-}sec,\lambda}$ equals the cross section of the specimen in zone between two temperature sensors.

While some of the aforementioned factors are measuring errors (temperature gradient, power applied, geometry) others are process errors (heat losses definition, unsteady effects). Tab. 1 lists the most important sources of error and assigns to them a corresponding absolute and relative error. With Eq. 1 the maximal relative error of the heat conductivity measurements (without considering potential heat losses) calculates as follows:

$$\frac{\frac{\Delta\lambda_{eff,1-D}}{\lambda_{eff,1-D}}}{} = \frac{\Delta Q_{applied}}{Q_{applied}} + \frac{\Delta L_{sensors}}{\Delta L_{sensors}} + \frac{\Delta F_{cross-sec}}{F_{cross-sec}} + \frac{\Delta(\Delta T_{sensors})}{\Delta T_{sensors}} \qquad (3)$$

Hence, the maximal relative error considering the values from Tab. 1 is ±0.14. The highest impact on the relative error in the thermal conductivity measurement has the applied heat, closely followed by the cross-section area of the sample and the temperature difference between the two relevant sensors.

3.2. Results thermal conductivity measurement

Tab. 2 lists the temperature readings along the CFRP rod and the corresponding temperature differences between each sensor pairing (#n) - (#n+1). It shows that the heat flux applied to the CFRP rod creates in steady-state condition, id est $\Delta T_{sensor} \leq \pm 0.05$ K/h for each sensor, a constant temperature decrease. This is in accordance with the expectation for the quasi-homogenous material properties in the rod's longitudinal axis and equidistant sensor positions. The temperature decrease between each sensor pairing is in average 0.55 K and in total 2.77 K between sensor $TS_{\#4}$ and $TS_{\#9}$. Hence, with a heat flux of 704 W/m² passing through a cross section of $F_{cross\text{-}sec,\lambda} = A_{rod} = 5\text{x}10$ mm², the resulting thermal conductivity is $\lambda_{eff,1\text{-}D} = 38.1$ W/(m*K) ±5.3 W/(m*K) at an average temperature of 28.2 °C. The theoretical thermal conductivity of the rod calculates to 37.15 W/(m*K) at 25 °C [2]. This is a very good agreement and confirms that the experimental setup is capable delivering a reasonable temperature gradient measurement.

Table 1: Factors influencing the heat conductivity measuring results and assigned errors.

Parameter	Variable	Unit	Value A	Absolute error ±ΔA	Relative error ±ΔA/A
Heat flux density in flux sensor	q	W/m²	704	21.12	0.03
Heater flange dim. 1	L1	m	0.01	0.00005	0.005
Heater flange dim. 2	L2	m	0.01	0.00005	0.005
Cross section for heat flux through heater	$F_{cross\text{-}section,q}$	m²	0.0001	$4*10^{-6}$	0.01
Applied heat	$Q_{applied}$	W	0.0704	0.002816	0.04
Distance between temperature sensors	$\Delta L_{sensors}$	m	0.075	0.0005	0.0067
Sample height	H	m	0.005	0.0001	0.02
Sample width	W	m	0.01	0.0001	0.01
Cross section of sample	$F_{cross\text{-}section,\lambda}$	m²	0.5*10-4	$1.5*10^{-6}$	0.03
Temperature	T	K	300	0.05	
Temperature difference between sensors	$\Delta T_{sensors}$	K	2.74	0.1	0.036

Table 2: Temperature readings [°C] along the CFRP rod and resulting temperature gradients. Boundary conditions: 704 W/m², 25 °C.

Temp. sensor No.	#4	#5	#6	#7	#8	#9	#14
$T_{meas.}$	29.64	29.06	28.48	27.95	27.44	26.78	24.96
$\Delta T_{\#n\text{-}\#(n+1)}$	---	0.58	0.58	0.53	0.51	0.57	n.a.

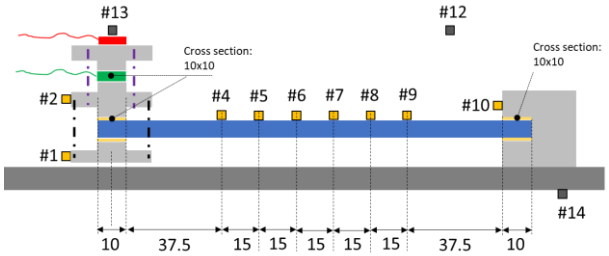

Figure 3: CFRP rod (blue) with applied Pt-100 sensors (orange). Dark grey coloured sensors are out of calibration. In red the resistance heater, in green the heat flux meter and in light yellow conductive pads. Thermal insulation is not depicted.

4. SINGLE-LAP JOINT THERMAL GRADIENT MEASUREMENT

The second part of the paper refers to the single-lap joint experiment. The goal is to determine the temperature distribution along two CFRP rods that are single-lap joined over a length of 20 mm (cf Fig. 5) and to compare the measurement with a finite element simulation. From this also the heat flux distribution in the joint can be derived, though, this is not of concern in the present paper.

The adherends' cross section and material properties (i.e. layup) is the same as for the rod used for the thermal conductivity measurement in paragraph 3. Only the length is with 150 mm each slightly shorter. Again, the boundary conditions are controlled by several temperature sensors. $TS_{\#1}$ and $TS_{\#18}$ measure the hot and cold flange temperature, respectively; $TS_{\#20}$ the shroud, $TS_{\#17}$ the resistance heater temperature and $TS_{\#19}$ the heat flux flange. In difference to the thermal conductivity setup, the control sensor for the single-lap joint experiment is $TS_{\#2}$. This allows a more precise setting of the temperature boundary condition to 25°C +/-0.1°C, as it does not involve the contact resistance between cold flange and cold plate. Another difference is the sensor type: Thin film Pt100 1/3 DIN class B, 2x5 mm, 4-wire connection. The sensors are applied on both sides of the specimen, id est $TS_{\#4}$…$TS_{\#10}$ on the top site and $TS_{\#11}$…$TS_{\#16}$ on the bottom side. This is especially required in the jointed area with a temperature gradient in thickness direction. "Before" and "after" the joint the heat flux distribution is expected to be one-dimensional. Thus, comparing the sensor readings on top and bottom side allows to inherently proof check the one-dimensionality, because the couples $TS\#_{4\text{-}11}$, $TS\#_{5\text{-}12}$ as well as $TS_{\#9\text{-}15}$ and $TS_{\#10\text{-}16}$ are expected to deliver the same reading. At the same time, both pairings are positioned at a same distance of 20 mm from each other. Assuming no heat losses, both pairings will show the same temperature gradient. The clamping at hot and cold flange is the same as for the single rod (cf. Fig. 1).

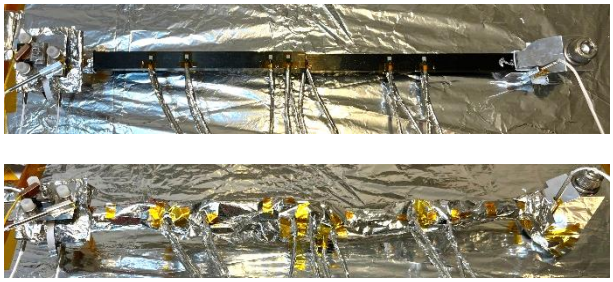

Figure 4: Experimental setup of single-lap joint on cold plate without (top) and with (bottom) SLI wrapping. A separate SLI (not shown) is enclosing the heater flange.

4.1. Comparison of simulation and experimental results for single-lap joint

The finite element model (MSC Patran/Nastran) used in the simulation is depicted in Fig. 6. It consists only HEX8 elements, which are refined in the jointed area. In between the two adherends a layer of 0.1 mm glue is simulated as well as the conductive pads (Kerafol® 86/300) at each contact surface between the adherends and the flanges. While the elements representing the CFRP feature a transversal isotropic material properties (MAT5), the glue and conductive pad layers feature isotropic properties (MAT4). The magenta and red marks represent the total heat (QBDY3) and temperature (SPC) boundary condition, respectively. Both are applied symmetrically to the flanges. The solution (SOL 153) is obtained for the steady state case (cf Fig. 7). In the experiment, the temperature distribution in the single-lap joint is determined by setting the reference cold flange temperature ($TS_{\#2}$) to 25°C +/- 0.1°C and the added heat via the resistance heater to 0.1 W. The actually measured heat at the heat flux sensor is 0.0788 W, which again is applied as heat boundary condition in the simulation.

This results in the simulated and measured temperature distribution which is listed in Tab. 3. The first row indicates the experimental readings under the above-mentioned boundary conditions and the second one calculates the corresponding ΔT: $TS_{\#4}$-$TS_{\#5}$ and $TS_{\#11}$-$TS_{\#12}$ as well as $TS_{\#9}$-$TS_{\#10}$ and $TS_{\#15}$-$TS_{\#16}$. The third row lists the results from

the FE simulation. Especially for $TS_{\#4}$-$TS_{\#5}$ and $TS_{\#11}$-$TS_{\#12}$ the temperature gradient is quite different in the measurements. While $TS_{\#4}$-$TS_{\#5}$ is close to the simulated gradient, $TS_{\#9}$-$TS_{\#10}$ is reduced by a factor of approx. two. Based on the material's measured thermal conductivity of λ_{eff} = 38.1 W/(m*K) ±5.3 W/(m*K), cf paragraph 3, the temperature gradient should be for both sensor pairs in the range of ΔT =0.7…1 °C. Also, the overall temperature level is significantly higher in the simulation than in the actual measurements.

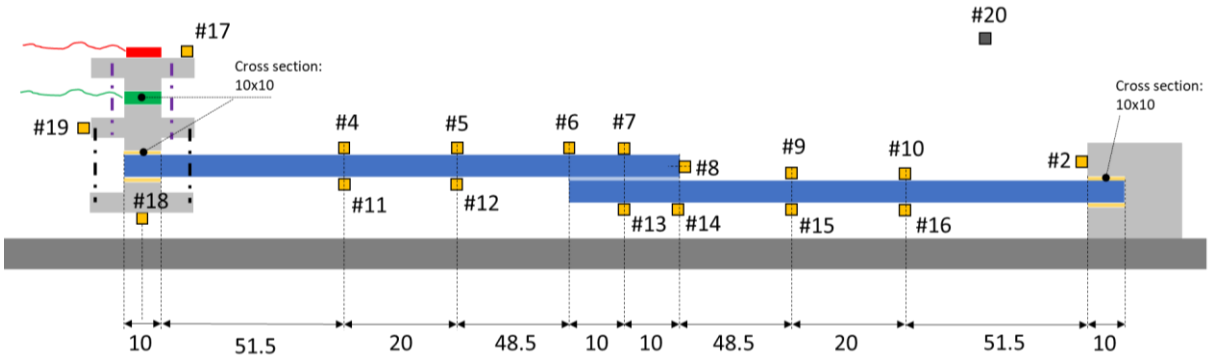

Figure 5: Single lap joint specimen made of CFRP rods (blue) with applied Pt-100 sensors (orange). Dark grey coloured sensors are out of calibration. In red the resistance heater and in green the heat flux meter. Thermal insulation is not depicted.

Table 3: Results of the measured and simulated temperature [°C] distribution along the SLJ specimen.

Temp. sensor No.	**#4 #11**	**#5 #12**	**#6**	**#7**	**#8**	**#13**	**#14**	**#9 #15**	**#10 #16**	**#18**	**#19**	**#20**
$T_{meas.}$ (@ Q=0.788 W)	30.9 30.9	30.2 30.3	28.9	28.7	28.6	27.6	27.5	26.7 26.7	26.4 26.3	33.3	33.6	24.7
$\Delta T_{\#(n-1) - \#n}$	---	0.7 0.6	---	---	---	---	---	---	0.3 0.4	---	---	---
$T_{sim.}$	35.15 35.15	34.32 34.32	32.51	32.32	32.05	30.57	30.38	28.57 28.57	27.74 27.74	37.85	37.85	n.a.

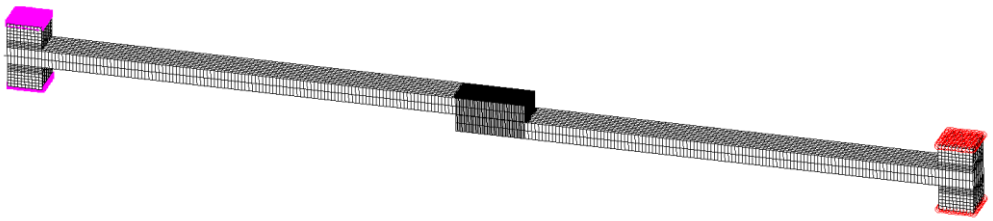

Figure 6: FE model of single lap joint with highlighted boundary conditions. Magenta: Q_{total}=0.0788 W, Red: $T_{coldplate}$=298.15K.

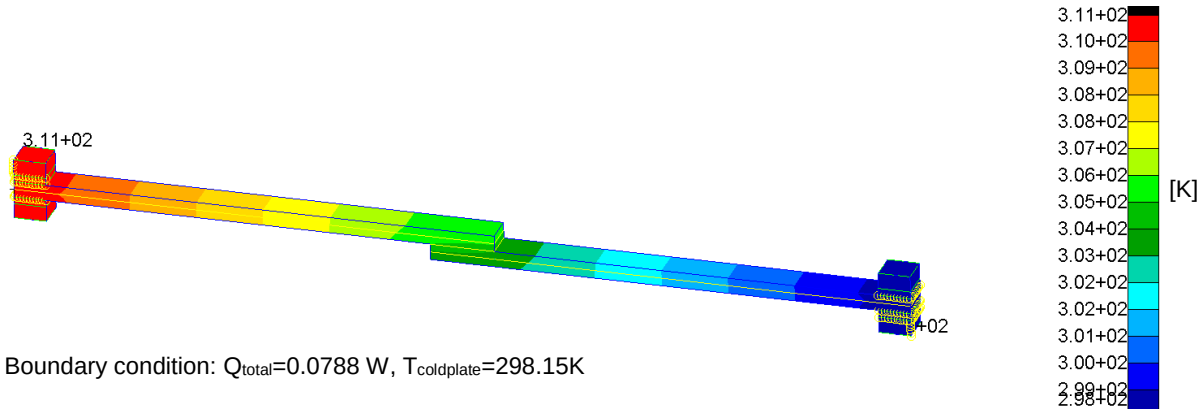

Figure 7: Temperature distribution [K] in FE simulation (excl. radiation).

This indicates that there is a major underlying phenomenon that is not correctly considered in the experiment and/or simulation, yet. The hypothesis is that radiation effects still play a very important role. In comparison to the single-lap joint experiment, the additional (inner) MLI, cf Fig. 2, is missing. In order to investigate and quantify this influence, a simplified analytical approach is used. It is assumed that the shroud, covered from the inside with SLI, behaves like an infinite space when it is faced by the specimen. Hence, for two grey bodies with the surrounding one sufficiently larger than the enclosed one the net heat transfer from the specimen to the shroud simplifies as follows [3]:

$$Q = A \cdot \sigma \cdot \varepsilon_{rod} \cdot (T_{rod}^4 - T_{shroud}^4) \qquad (4)$$

Here, A is the surface of the CFRP rod, σ is the Stefan-Boltzmann constant, ε_{rod} the emissivity of the CFRP rod and T the (local) temperature of the rod and the shroud, respectively. As the rod is wrapped in SLI the emissivity is significantly reduced. Initially we assume that the effective emissivity of the CFRP rod wrapped in SLI is $\varepsilon_{rod,eff} = \varepsilon_{SLI} = 0.15$. The emissivity of the heater flange, also wrapped in SLI, is assumed as $\varepsilon_{SLI,flange} = 0.1$. Next, the specimen is subdivided in four sections (cf Fig. 8) in order to determine a local arithmetic mean temperature at which each section radiates. It is calculated for each section on the basis of the two and four depicted Pt100 sensors (orange), respectively.

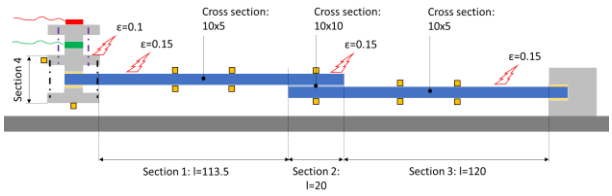

Figure 8: Sections with assigned emissivity and temperature sensors (orange) for radiation calculation.

From the temperature readings in the experiment (cf Tab. 3) the mean temperatures are $T_{Sect.1}$ = 30.61°C, $T_{Sect.2}$ = 28.22°C, $T_{Sect.3}$ = 26.56°C and $T_{Sect.4}$ = 37.85°C. Hence, the radiated heat Q_{rad} from the rod and the flange to the shroud calculates with Eq. 4 for section 1 to section 4 as listed Tab. 3. $Q_{applied}$ = 0.0788 W is the actually applied heat measured by the heat flux meter. It is noticed that a quite large part of the applied heat is radiated at the flange in section 4 (13.2%) and in the first half of section 1 (23.7%). This corresponds to the expectation, because the larger temperature gradient of the sections closer to the heater results in a larger heat radiation towards the shroud. With the remaining heat $Q_{eff,i}$ reaching effectively the two sensor pairs $TS_{\#4}$-$TS_{\#5}$ and $TS_{\#9}$-$TS_{\#10}$, the effective thermal conductivity λ_{eff} is calculated. For example, $Q_{eff,1}$ = (0.0788 - 0.0104 - 0.5 · 0.0178) W = 0.0591 W and $Q_{eff,3}$ = (0.0788 - 0.0104 - 0.0178 - 0.0026 - 0.5 · 0.0061) W = 0.0591 W. Considering a mean temperature drop at both sensor pairings of 0.7°C and 0.35°C (Tab. 3) in section 1 and section 3, respectively, the effective thermal conductivity calculates with Eq. 1 in section 1 to $\lambda_{eff,Sect.1}$ = 30.8 W/(m*K) and in section 3 to $\lambda_{eff,Sect.3}$ = 44.5 W/(m*K). This is physically still not right, because both adherends are made from the same material and have consequently the same thermal conductivity.

Table 4: $\varepsilon_{SLI} = 0.15$ and $\varepsilon_{SLI,flange} = 0.1$, $Q_{applied}$ = 0.0788 W

Section i	$Q_{rad,i}$ [W]	$Q_{rad,i}$ / $Q_{applied}$ [-]	$Q_{eff,i}$ [W]	λ_{eff} [W/(m*K)]
4	0.0104	0.132	---	---
1	0.0187	0.237	0.0591	30.8
2	0.0026	0.033	0.0484	---
3	0.0061	0.077	0.0441	44.5

Hence, the emissivity of the SLI covering the adherends and the one wrapping the flange is iteratively changed until the same conductivity is reached for both adherends. As demonstrated in Tab. 5, this is the case when $\varepsilon_{SLI} = 0.26$ and $\varepsilon_{SLI,flange} = 0.1$. The corresponding effective thermal conductivity is then in both sections approximately λ_{eff} = 29.8 W/(m*K).

Table 5: $\varepsilon_{SLI} = 0.26$ and $\varepsilon_{SLI,flange} = 0.1$, $Q_{applied}$ = 0.0788 W

Section i	$Q_{rad,i}$ [W]	$Q_{rad,i}$ / $Q_{applied}$ [-]	$Q_{eff,i}$ [W]	λ_{eff} [W/(m*K)]
4	0.0104	0.132	---	---
1	0.0324	0.411	0.0522	29.8
2	0.0045	0.057	0.0338	---
3	0.0106	0.135	0.0262	29.9

Even though, this conductivity value is lower than expected and only one power set point is evaluated up to the point of writing, we conclude from the analytical approximation that there still exists a significant radiative heat leak in the current setup. This prevents us from measuring the exact temperature distribution (due to conduction only) along the single-lap joint. In order to minimize the radiative heat leak, it is suggested to wrap both, the specimen and the heater flange, not only in SLI, but in MLI. Another option is a dedicated section-wise temperature-controlled shroud along the specimen. Further the heat flux sensor could be installed directly on the specimen in order to remove also the influence of the $Q_{rad,4}$ on $Q_{applied}$ when not properly radiation shielded.

5. SUMMARY AND OUTLOOK

We have presented two experimental setups, one

for measuring the thermal conductivity $\lambda_{11} = \lambda_{eff, 1\text{-}D}$ of a CFRP rod (M40J-UD/MTM46, f_{vol}=54%) and one to measure the temperature distribution along a single-lap joint of the same material. Both setups include improvements over an earlier test setup [2]. These are mainly the inclusion of a heat flux meter and an increased specimen geometry. The measurement of the thermal conductivity showed with λ_{eff} = 38.1 W/(m*K) ±5.3 W/(m*K) good results compared to an analytical calculation based on the material properties. Thus, the general setup including the added heat flux meter is validated, too.

The single-lap joint experiment showed quite some differences between the simulated and measured temperature distribution. The hypothesis is that the measurement is significantly affected by parasitic radiative heat losses from the specimen to the environment (shroud). An analytical approximation demonstrated this phenomenon in principal. However, it is not entirely conclusive as only one power set point is evaluated up to the point of writing. In any case, the setup cannot be used as is in order to measure accurately enough the temperature distribution along the CFRP SLJ.

We identified several possible improvements in the measurement setup in order to reduce the parasitic radiative heat flux. This includes the addition of MLI layers or a temperature-controlled shroud around the specimen and the flange. Further the heat flux meter could be positioned directly between a flange and the specimen, which will reduce possible remaining radiation effects on the measured heat flux considered for the experimental evaluation. At last, the calculation method of the parasitic heat flux itself and its implementation in the results processing as well as in the FE simulation can be refined.

ACKNOWLEDGMENTS

We would like to thank to our two colleagues Kaname Sasaki and Eugen Mikulz, both from DLR Institute of Space Systems, Bremen, for their great test support and discussion to further improve the test setup.

6. REFERENCES

1. M. Lange, V. Baturkin, C. Hühne, O. Mierheim (2018). Validation of an analytical model describing the heat flux distribution in load-bearing CFRP single-lap joints_v1. In Proc. of 15th European Conference on Spacecraft Structures, Materials & Environmental Testing, Noordwijk, The Netherlands.

2. M. Lange, V. Baturkin, C. Hühne, O. Mierheim (2016). Simulation and measurement of thermal fluxes in load-bearing bonded FRP single-lap joints. In Proc. of 14th European Conference on Spacecraft Structures, Materials & Environmental Testing, Toulouse, France.

3. John H. Lienhard IV. and John H. Lienhard V. (2018). A heat transfer textbook. Fourth Edition. Phlogiston Press. Cambridge, MA.